Received: 9 February 2023 | Revised: 17 April 2023 | Accepted: 21 April 2023

Micro & Nano Letters

DOI: 10.1049/mna2.12163

The Institution of Engineering and Technology WILEY

LETTER

Controllable synthesis of indium oxide nanorod-flowers for high field emission performance

Yuechuan Hu[1] | Hange Feng[1] | Lingwei Li[1] | Menghao Luo[1] | Zibo Dong[1] | Shaolin Xue[1,2]

[1]College of Science, Donghua University, Shanghai, P. R. China

[2]Shanghai Institute of Intelligent Electronics and Systems, Donghua University, Shanghai, P. R. China

Correspondence
Shaolin Xue, College of Science, Donghua University, Shanghai 201620, P. R. China.
Email: slxue@dhu.edu.cn

Funding information
Fundamental Research Funds for the Central Universities; Graduate Student Innovation Fund of Donghua University, Grant/Award Number: CUSF-DH-D-2021049

Abstract

In this paper, indium oxide (In_2O_3) nanomaterials are successfully synthesized on the silicon substrates by hydrothermal method and calcination. By changing the ratio of raw materials, In_2O_3 exhibits three morphologies of nanorods, nanomaces, and nanorod-flowers. Among the three morphologies of In_2O_3 nanomaterials, the nanorod-flowers shaped In_2O_3 shows a strong field emission property, the turn-on electric field as low as 0.97 V/μm and the field enhancement factor β up to 1053. The excellent performance is attributed to the higher length to diameter (L/D) ratio of the emitting tips and the better crystal quality for nanorod-flowers shaped In_2O_3. The authors also show that for the nanorod-flowers shaped In_2O_3, increasing separation distance, the turn-on electric field increases up to about 3.67 V/μm and β decreases to 573 at $d = 900$ μm. This work provides new insights to design and synthesize nanomaterials with excellent field emission properties.

1 | INTRODUCTION

Field emission is a quantum tunnelling process in which electrons around the Fermi energy level escape from the surface of the material under the strong external electric field (about 10^5 V/cm) [1]. It has attracted an increasingly interests of researchers for its enormous applications in communication satellites, microwave devices, space research, X-ray sources and display light sources [2–4]. Field emission-related electronic devices must possess excellent electron emission properties, for instance, low turn-on electric field, strong field enhancement factor, high density and stability of field emission current, which require strict demands on the materials' composition, nanostructure, size of morphology, crystallization, and the tip shielding effect.

At present, a large number of cathode-emitting materials have been explored and developed, such as ZnO [5], SnO_2 [6], SiC [7], GaN [8], graphene [9, 10], etc. With the research advanced, several methods emerged to improve the field emission behaviour: (1) letting the emitting materials to grow into sharp curvature tips [11—13]; (2) decreasing the work function (ϕ), at the same time raising the electrical conductivity of the nanomaterials [14—16]; (3) modifying the crystallinity of nanomaterials for the effective charge transfer [17]. During the above improving methods, the first method is a simple way to improve the field emission properties. Increasing the length to diameter (L/D) ratio is a crucial way to obtain the sharp emitters, it means that decreasing the diameter or increasing the length of the emitting tip.

Indium oxide (In_2O_3), a wide bandgap semiconductor with a direct bandgap of about 3.6 eV [18], has attracted widespread attention, due to its high electrical conductivity, low electron affinity, strong chemical stability, and easily controllable shape [19, 20]. In this work, using the hydrothermal method combined with high-temperature calcination, we successfully synthesized the In_2O_3 nanomaterials with different L/D ratios. The nanorod-flower shaped In_2O_3 with the higher L/D ratio possesses the lower turn-on electric field (0.97 V/μm) and the stronger field enhancement factor (1053), thus providing an optimal field emission performance.

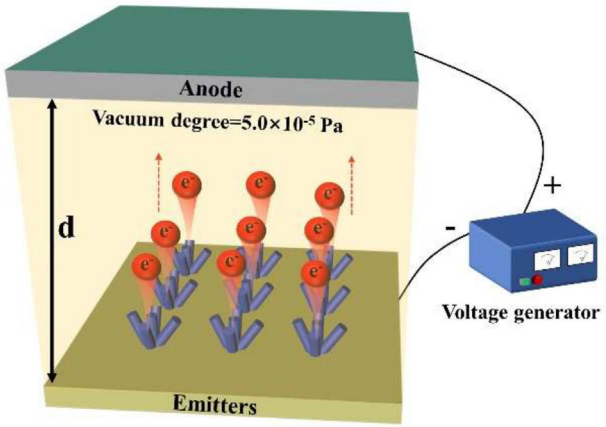

FIGURE 1 Scheme of the FE experimental setup.

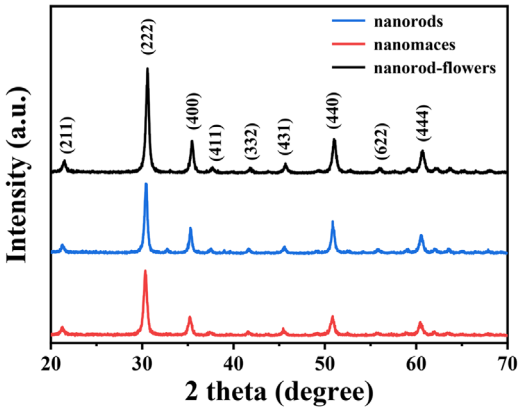

FIGURE 2 XRD patterns of the obtained In_2O_3 nanorods, nanomaces, and nanorod-flowers. In_2O_3, indium oxide.

2 | EXPERIMENTAL SECTION

2.1 | Growth of In_2O_3 nanomaterials on the silicon substrate

Firstly, the obtained In_2O_3 suspension with different ingredient ratios (indium chloride:urea:glucose) was uniformly deposited on the washed silicon substrates. Subsequently, the silicon substrates deposited with In_2O_3 were put into an autoclave and heated at 180°C for 24 h. Then the autoclave cooled down to the room temperature. The silicon substrates were rinsed and dried at 60°C. Lastly, the obtained samples were transferred into an atmosphere furnace and calcined at 700°C for 2 h in air.

2.2 | Field emission performance experiments

The CS-180 field emission performance instruction was used to study the field emission performance of the In_2O_3 nanomaterials in a vacuum environment of 5.0×10^{-5} Pa with a structure of double parallel flat plates, as shown in Figure 1. An ITO glass and the In_2O_3 nanomaterials were used as the anode and cathode, respectively, and the distance from the cathode to the anode material was controlled at 300, 600, and 900 μm, and the maximum range of the applied voltage was 0 to 3500 V. The currents were collected every 10 V to examine the field emission performance of In_2O_3 nanomaterials by a Keithley 6430 unit.

The other particular experiments and characterization could be found in Supplementary information.

3 | RESULTS AND DISCUSSION

Figure 2 shows the representative XRD patterns of the three In_2O_3 nanostructures. The characteristic diffraction peaks are located at 30.43°, 35.29°, 50.94°, and 60.58° corresponding to the (222), (400), (440), and (622) faces of cubic In_2O_3 (JCPDS 06–0416). And no other characteristic diffraction peaks are found in the spectra, indicating the high purity of In_2O_3 nanomaterials. Moreover, compared with nanorods and nanomaces, the characteristic peaks of nanorod-flowers like In_2O_3 exhibit a stronger intensity which certifies the excellence of crystal quality.

Figure S1 displays the SEM images of $In(OH)_3$ in different ingredient ratios and different reaction times. The calcined In_2O_3 nanomaterials present the same structures compared to $In(OH)_3$. The In_2O_3 with ingredients ratio of 1:4:6 shows a nanorod structure, as shown in Figure 3a. Figure 3b exhibits that the In_2O_3 with an ingredients ratio of 1:4:4 possesses a nanomace structure. At the ingredients ratio of 1:8:4, the In_2O_3 presents the nanorod-flowers structure, as shown in Figure 3c. The lengths of In_2O_3 nanorods, nanomaces, and nanorod-flowers are all about 1 μm. Besides, the radii of them are about 75, 125, and 50 nm, respectively. The TEM images of nanorod-flowers shaped In_2O_3 are shown in Figure 3d. The rods are generally uniform and straight. Meanwhile, the length of the rod is about 1 μm and the radius is approximately 50 nm. The HRTEM image (Figure 3e) represents that the nanorod-flowers shaped In_2O_3 have the lattice fringes with an interlayer distance of 0.292 nm, corresponding to the (222) crystal plane of c-In_2O_3 [21]. The elements composition of In_2O_3 nanorod-flowers was further evidenced by EDS in Figure 3f. It shows that the sample consists of In, O together with minor Si, C, and Pt elements. The atomic ratio of In to O is near 2:3, revealing that they are In_2O_3. The possible formation process of the In_2O_3 nanomaterials is shown in Figure S2.

The field emission properties of the In_2O_3 nanostructures have been investigated under 5.0×10^{-5} Pa at the room temperature for different cathode–anode separation distances. Their current density (J) as a function of electric field (E) in the distance of 300 μm is shown in Figure 4a. J is calculated based on the current (I) divided by emission area (S), and E stands for the voltage (V), which is divided by the separation distance (d) of the anode and the cathode. Here, we define the electric fields for generating the current densities of 1 μA cm^{-2} as the turn-on field [1]. The turn-on electric fields (Eon) of In_2O_3 nanorods, nanomaces, and nanorod-flowers are 4.05, 4.5, and 0.97 V/μm, respectively. From Figure 4a, the experimental data are plotted

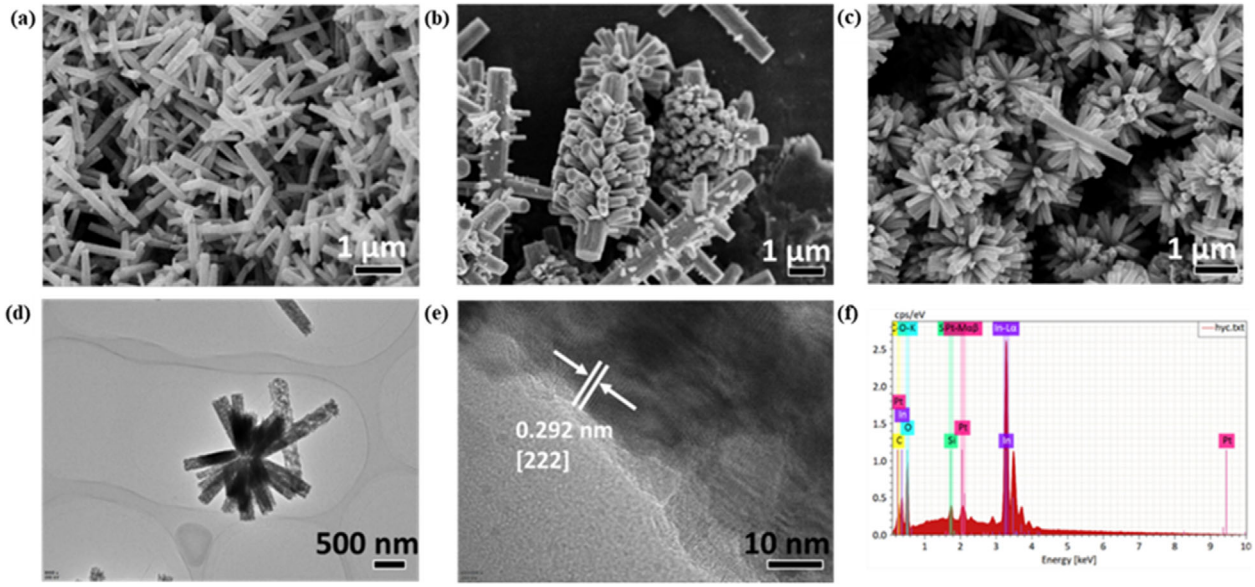

FIGURE 3 SEM images of In_2O_3 nanomaterials: (a) nanorod structure, (b) nanomace structure, and (c) nanorod-flowers structure; (d) TEM and (e) HRTEM images of nanorod-flowers shaped In_2O_3; (f) EDS spectrum of nanorod-flowers shaped In_2O_3. In_2O_3, indium oxide.

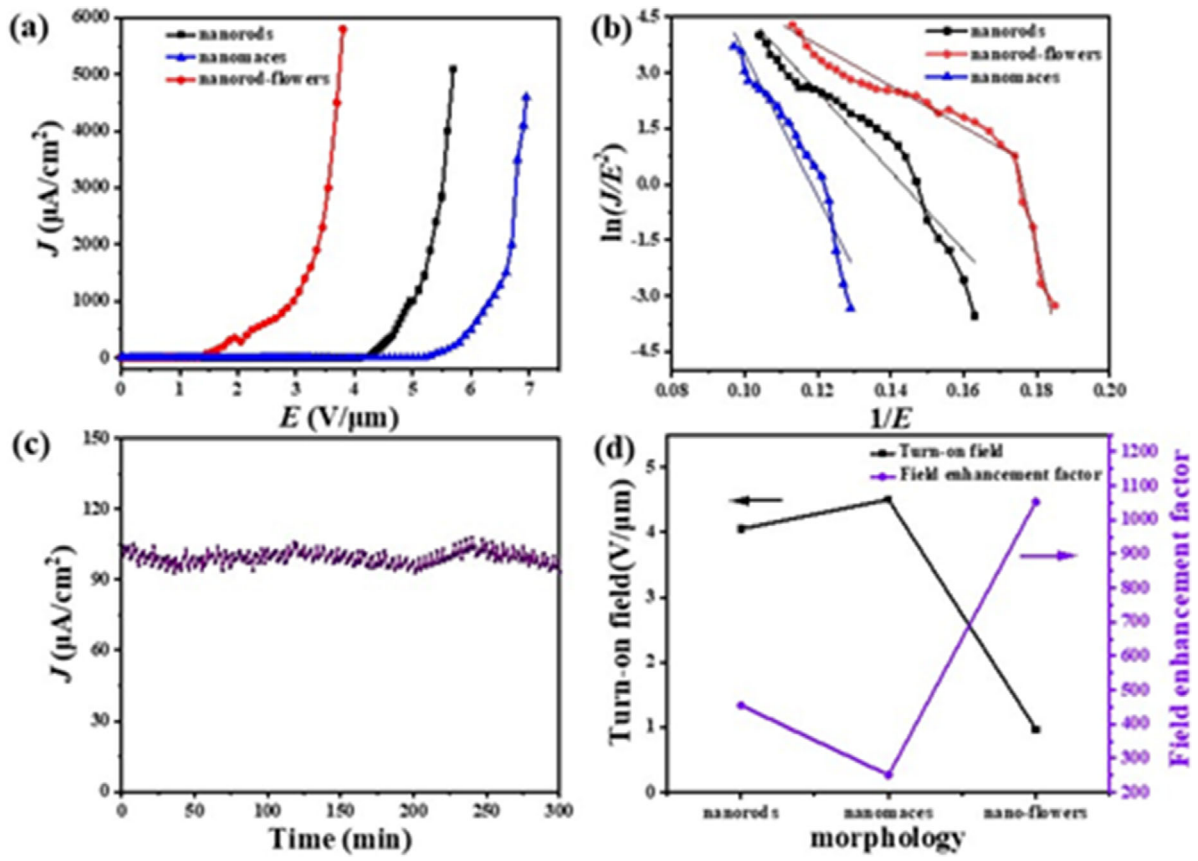

FIGURE 4 (a) Typical J–E curves of three In_2O_3 nanostructures. (b) Their corresponding F–N plots and linear fittings (solid lines). (c) Their electron emission stability under 1.55 (V/μm). (d) The variations of E_{on} and β with the changing of morphology. In_2O_3, indium oxide.

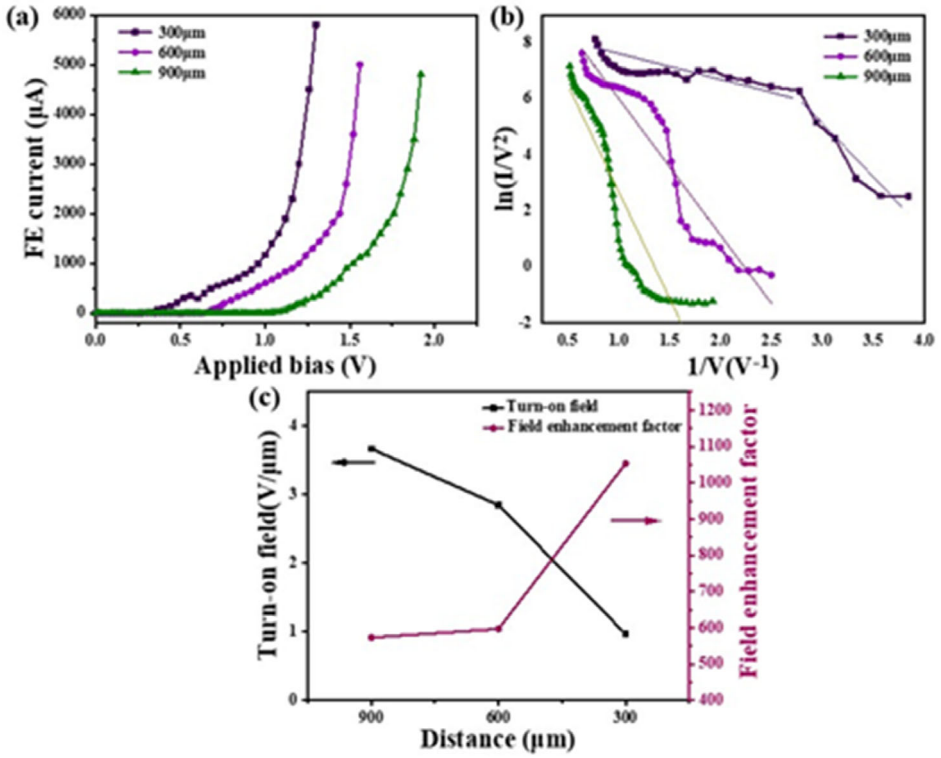

FIGURE 5 (a) Field emission *I–V* characteristics of nanorod-flowers shaped In_2O_3 for various cathode–anode separation distances plotted on a linear scale. (b) FN plots corresponding to the *I–V* curves and linear fittings (solid lines). (c) The variations of E_{on} and β with the changing of distance. FN, Fowler–Nordheim; In_2O_3, indium oxide.

in order to visualize the current rising better. It is clear that the FE current exponentially grows as an exponential function and raises up about six orders of magnitude, and the nanorod-flowers shaped In_2O_3 exhibits the highest current emission density. It indicates that the larger L/D ratio of the sample possesses the better field emission performance. To analyze the FE characteristics deeply, we refer to the Fowler–Nordheim (FN) theory. The FN theory has proven to be a valid model for achieving a first-approximation understanding of the emission phenomena from several nanostructures. It is shown below [22]

$$J = A(\beta^2 E^2)/\phi exp(-(B^{(3/2)})/\beta E) \quad (1)$$

$$ln(J/E^2) = -(B\phi^{(3/2)})/\beta E + ln((A\beta^2)/\phi) \quad (2)$$

where J is the emission current density, E suggests electric field, $A = 1.54 \times 10^{-6}$ (AV^{-2} eV), $B = 6.83 \times 10^3$ ($V(eV)^{-3/2}$ μm^{-1}), β indicates the field enhancement factor, reflecting the enhancement of the field emission of any sharp edges or emitting tips over the flat plane, ϕ is the work function of In_2O_3 (3.7 eV) [23]. The corresponding FN plots of the three emitters are shown in Figure 4b. The F–N curves of all three structures of In_2O_3 show a linear feature in which $\ln(J/E^2)$ is plotted as a function of $1/E$, indicating that the electron emission process follows the field emission mechanism originated from the quantum tunnelling effect [24]. By using the slope of the F–N plot obtained from the numerical fitting, we can calculate the field enhancement factor β. The obtained β values of the prepared In_2O_3 nanorods, nanomaces are calculated as 251 and 455, respectively. However, we have found that for the nanorod-flowers shaped In_2O_3, a double slope in the F–N plot is observed and we estimate a field enhancement factor $\beta = 200$ for the low bias region and $\beta = 1053$ for the high bias region. To explain the existence of two different β, one at low bias corresponding to a smaller field enhancement factor, and one at high bias corresponding to the larger one, we need to take into account the rod-shaped emitters with an irregular growth orientation. At low voltages, only emitters grown vertically to the silicon substrate start the emission process and reflect good field emission properties. With the voltage increasing, the other emitters begin to contribute to the emitted current. The nanorod-flowers shaped In_2O_3 emitters were also performed at 1.55 V/μm. The fluctuation at a current density value of nanorod-flowers shaped In_2O_3 is about 7% over 300 min, indicating the outstanding stability of the emission current, as shown in Figure 4c. In addition, Figure 4d presents an alteration of the field emission parameters of the nanomaterials with different morphologies. These results demonstrate that the larger the L/D ratio of the In_2O_3 emitters, the better the field emission performance.

Moreover, we have also performed a study of the field emission's properties as a function of the distance d by varying the cathode–anode separation distance at 300, 600, and 900 μm. In the case of nanorod-flowers shaped In_2O_3, the *I—-V* characteristics measured for different d values are shown in Figure 5a. Indeed, for $d = 300$ μm, $d = 600$ μm, and $d = 900$ μm, the turn-on electric fields are 0.97, 2.85, and 3.67 V/μm, separately.

TABLE 1 Comparison of the turn-on fields from some previously reported In_2O_3 emitters and this work.

Emitters	E_{on} (V/μm)	References
In_2O_3 nanoneedles	4.90 (10 μA/cm^2)	[1]
In_2O_3 nanocolumn	3.20	[18]
In_2O_3 nanoflowers	3.54	[24]
In_2O_3 nanowires	7.00	[12]
MoS_2 nanoflowers	12.00	[26]
SnO_2 nanoflowers	2.60 (0.1 μA/cm^2)	[27]
β-Ga_2O_3 nanopillars	30.00 (100 A/cm^2)	[28]
GaN	—	[29]
In_2O_3 nanorod-flowers	0.97	Our work

In_2O_3, indium oxide.

Similarly, for each curve shown in Figure 5a we also reported the F–N plot in Figure 5b. According to the following equation, the emitted current as a function of distance can be expressed as [25]

$$I = SA\phi^{-1}(\beta V/d)^2 exp[-B\phi^{(3/2)}(\beta V/d)^{-1}] \quad (3)$$

where S is the effective area from which electrons are field emitted. The slope of the linear FN fitting is used to extract the field enhancement factor β under different cathode–anode separation distances, and the values being $\beta = 573$ and $\beta = 597$ for $d = 900$ μm and $d = 600$ μm, respectively. Then, the data are reported in Figure 5c; we observe very similar behaviour that the turn-on voltage is increased monotonically by increasing the separation distance and the field enhancement factor results to be a decreasing function of the distance d. Consequently, field emission parameters, such as turn-on field and field enhancement factor, showed monotonic dependence when the cathode–anode separation distances are at 300, 600, and 900 μm.

As shown in Table 1, we summarize the turn-on fields of some previously reported In_2O_3 emitters as well as emitters of similar shape and some wide bandgap semiconductor emitters compared with ours. We achieved low turn-on voltage of In_2O_3 nanomaterial emitters.

4 | CONCLUSION

In summary, we reported the controllable synthesis of In_2O_3 nanomaterials on silicon substrates through the hydrothermal combined with calcination. The effect of the concentration of glucose and urea in the reaction solution on the morphology and FE properties of In_2O_3 was investigated. It was found that In_2O_3 nanorod-flowers possess the higher L/D ratio of the field emission tips and better crystal quality with the lower turn-on electric field of 0.97 V/μm and a stronger field enhancement factor of 1053. We also found that the turn-on field and the field enhancement factor showed monotonic dependence when the cathode–anode separation distance was in the range (300, 600, and 900 μm). This provides a new thought to realize the controllable synthesis of nanomaterials for different field emission devices.

AUTHOR CONTRIBUTION

Hu, Yuechuan: Investigation, Methodology, Writing—original draft, Writing—review & editing; **Feng, Hange**: Methodology, Validation; **Li, Lingwei**: Investigation, Methodology; **Luo, Menghao**: Data curation, Visualization; **Dong, Zibo**: Conceptualization, Supervision; **Xue, Shaolin**: (Corresponding Author).

ACKNOWLEDGEMENTS

The work was supported by Fundamental Research Funds for the Central Universities and Graduate Student Innovation Fund of Donghua University (NO. CUSF-DH-D-2021049).

CONFLICTS OF INTEREST STATEMENT

The authors declare no conflict of interest.

DATA AVAILABILITY STATEMENT

The data that support the findings of this study are available from the corresponding author upon reasonable request.

ORCID

Shaolin Xue https://orcid.org/0000-0001-5876-7886

REFERENCES

1. Wang, B., Zheng, Z.Q., Wu, H.Y., Zhu, L.F.: Field emission properties and growth mechanism of In_2O_3 nanostructures. Nanoscale Res. Lett. 9, 111 (2014)
2. Ma, L.A., Wei, Z.H., Guo, T.L.: Improved field emission properties of Au nanoparticles and CNTs decorated SnO_2 nanowire arrays on carbon fibers. J. Mater. Sci. Mater. Electron. 27(9), 9044–9051 (2016)
3. Chen, L.L., Guo, L.W., Liu, Y., Li, Z.L., Huang, J., Lu, W.: A comparison of the field emission characteristics of vertically aligned graphene sheets grown on different SiC substrates. Chinese Phys. B. 22(10), 107901 (2013)
4. Nishida, S., Yamashita, T., Hasegawa, S., Asahi, H.: Barrier height control for electron field emission by growing an ultra-thin AlN layer on GaN/Mo. Thin. Solid Films. 464, 128–130 (2004)
5. Yang, S.H., Hsu, N.C.: Electron emission enhancement of long hybrid emitters prepared using ZnO nanowires decorated with Zn nanoflakes. Appl. Surf. Sci. 433, 639–646 (2018)
6. Giubileo, F., Faella, E., Pelella, A., Kumar, A., Capista, D., Passacantando, M., Kim, S.S., Di Bartolomeo, A.: SnO_2 nanofibers network for cold cathode applications in vacuum nanoelectronics. Adv. Electron Mater. 8(10), 2200237 (2022)
7. Jung, W., Oh, D.H., Song, I., Shin, H.C., Ahn, S.J., Moon, Y., Park, C.Y., Ahn, J.R.: Influence of graphene-substrate interactions on configurations of organic molecules on graphene. Pentacene/epitaxial graphene/SiC. Appl. Phys. Lett. 105(7), 071606 (2014)
8. Seo, H.W., Tu, L.W., Chen, M., Chen, Q.Y., Bensaoula, A., Wang, X.M., Chu, W.K.: GaN nanorod arrays as a high-stability field emitter. J. Korean Phys. Soc. 71(6), 340–344 (2017)
9. Giubileo, F., Di Bartolomeo, A., Iemmo, L., Luongo, G., Urban, F.: Field emission from carbon nanostructures. Appl. Sci. 8(4), 526 (2018)
10. Iemmo, L., Di Bartolomeo, A., Giubileo, F., Luongo, G., Passacantando, M., Niu, G., Hatami, F., Skibitzki, O.: Graphene enhanced field emission from InP nanocrystals. Nanotechnology 28(49), 495705 (2017)
11. Zhang, Y.A., He, L.C., Jin, T., Guo, T.L., Zhou, X.T., Lin, Z.X.: Surface-conducted field emission electron sources with ZnO emitters of different morphologies. J. Alloy. Compd. 688, 77–82 (2016)

12. Li, S.Q., Liang, Y.X., Wang, T.H.: Electric-field-aligned vertical growth and field emission properties of In_2O_3 nanowires. Appl. Phys. Lett. 87(14), 143104 (2005)
13. Zhang, Z.G., Wang, X.X., Zhang, J., Yu, M., Zhang, J.C., Zhang, H.D., Long, Y.Z.: Recent advances in 1D micro- and nanoscale indium oxide structures. J. Alloy Compd. 752, 359–375 (2018)
14. Ying, P.Z., Chen, S.L., Ren, X.L., Chen, Q.: Investigation of temperature on the field electron emission from flexible N-doped SiC nanoneedles. Superlattice. Microst. 86, 250–255 (2015)
15. Lv, Y.Y., Zhang, Z.Y., Yan, J.F., Zhao, W., Zhai, C.X.: Al doping influences on fabricating ZnO nanowire arrays: Enhanced field emission property. Ceram. Int. 44(7), 7454–7456 (2018)
16. Zhang, X.Q., Wang, C.W., Chen, J.B., Zhu, W.D., Liao, A.Z., Li, Y., Wang, J., Ma, L.: Enhancement of the field emission from the TiO_2 nanotube arrays by reducing in a $NaBH_4$ solution. ACS Appl. Mater. Interfaces 6(23), 20625–20633 (2015)
17. Gurylev, V., Chin, T.K., Useinov, A.: Charge transfer and field emission characteristics of TiO_2@CNTs nanocomposite: Effect of TiO_2 crystallinity. J. Alloy. Compd. 857, 157598 (2021)
18. Kar, S., Chakrabarti, S., Chaudhuri, S.: Morphology dependent field emission from In_2O_3 nanostructures. Nanotechnology 17(12), 3058–3062 (2006)
19. Lv, Y.K., Li, Y.Y., Zhou, R.H., Pan, Y.P., Yao, H.C., Li, Z.J.: N-doped graphene quantum dot-decorated three-dimensional ordered macroporous In_2O_3 for NO_2 sensing at low temperatures. ACS Appl. Mater. Interfaces 12(30), 34245–34253 (2020)
20. Liu, Y.Y., Liu, J.J., Pan, Q.J., Pan, K., Zhang, G.: Metal-organic framework (MOF) derived In_2O_3 and g-C_3N_4 composite for superior NO_x gas-sensing performance at room temperature. Sensor. Actuat. B Chem. 352, 131001 (2022)
21. Yue, L., Zhang, W.H., Zhang, W.D., Zhang, Q.F., Guan, R.F., Hou, G.H., Xu, N.: One-step solvothermal process of In_2O_3/C nanosheet composite with double phases as high-performance lithium-ion battery anode. Electro. Acta. 160, 123–130 (2015)
22. Sun, L., Ye, Z.F., Ma, L.A., Zhang, Y.A.: Improving field emission performance of patterned ZnO electron emission source by optimizing array spacing. Vacuum. 201, 111121 (2022)
23. Giubileo, F., Passacantando, M., Urban, F., Grillo, A., Iemmo, L., Pelella, A., Goosney, C., LaPierre, R., Di Bartolomeo, A.: Field emission characteristics of InSb patterned nanowires. Adv. Electron Mater. 6(10), 2000402 (2020)
24. Huang, Y.J., Yu, K., Zhu, Z.Q.: Controllable synthesis of novel In_2O_3 nanostructures and their field emission properties. Cryst. Res. Technol. 46(1), 90–94 (2011)
25. Giubileo, F., Bartolomeo, A.D., Zhong, Y., Zhao, S.R., Passacantando, M.: Field emission from AlGaN nanowires with low turn-on field. Nanotechnology 31(47), 475702 (2020)
26. Giubileo, F., Grillo, A., Passacantando, M., Urban, F., Iemmo, L., Luongo, G., Pelella, A., Loveridge, M., Lozzi, L., Di Bartolomeo, A.: Field emission characterization of MoS_2 nanoflowers. Nanomaterials 9(5), 717 (2019)
27. Zhang, Y.S., Yu, K., Li, G.D., Peng, D.Y., Zhang, Q.X., Xu, F., Bai, W., Ouyang, S.X., Zhu, Z.Q.: Synthesis and field emission of patterned SnO_2 nanoflowers. Mater. Lett. 60(25-26), 3109–3112 (2006)
28. Grillo, A., Barrat, J., Galazka, Z., Passacantando, M., Giubileo, F., Iemmo, L., Luongo, G., Urban, F., Dubourdieu, C., Di Bartolomeo, A.: High field-emission current density from β-Ga_2O_3 nanopillars. Appl. Phys. Lett. 114(19), 193101 (2019)
29. Litovchenko, V., Grygoriev, A., Evtukh, A., Yilmazoglu, O., Hartnagel, H.L., Pavlidis, D.: Electron field emission from wide bandgap semiconductors under intervalley carrier redistribution. J. Appl. Phys. 106(10), 104511 (2009)

SUPPORTING INFORMATION

Additional supporting information can be found online in the Supporting Information section at the end of this article.

How to cite this article: Hu, Y., Feng, H., Li, L., Luo, M., Dong, Z., Xue, S.: Controllable synthesis of indium oxide nanorod-flowers for high field emission performance. Micro Nano Lett. 18, 1–6 (2023). https://doi.org/10.1049/mna2.12163